2025 IEEE 26th Workshop on Control and Modeling for Power Electronics (COMPEL) | 979-8-3315-2702-0/25/$31.00 ©2025 IEEE | DOI: 10.1109/COMPEL57166.2025.11121220

Design of a Load Invariant Class-E Amplifier for an Inductively Heated Fluidized Bed

Rachel A. Hollett
Electrical Engineering
Stanford University
Stanford, CA 94305
rhollett@stanford.edu

Calvin H. Lin
Electrical Engineering
Stanford University
Stanford, CA 94305
calvinlin@stanford.edu

Dillon R. Jensen
Electrical Engineering
Stanford University
Stanford, CA 94305
dillonj0@stanford.edu

Jonathan A. Fan
Electrical Engineering
Stanford University
Stanford, CA 94305
jonfan@stanford.edu

Juan Rivas-Davila
Electrical Engineering
Stanford University
Stanford, CA 94305
jmrivas@stanford.edu

***Abstract*—This paper presents the design and implementation of a Class-E power amplifier invariant to both resistive and reactive load changes for inductively heating a fluidized graphite bed. The 66.5 V amplifier is capable of delivering up to 115 W to the varying load at 13.56 MHz. Tuned to the load impedance profile, the design utilizes a passive load transformation network to decrease the root mean square input current and compress output network phase angle variation to achieve zero-voltage switching across the entire load range.**

***Index Terms*—Power amplifier, induction heating, load invariant, fluidized bed, matching network**

I. Introduction

The push to reduce the carbon footprint of heavy industry has sparked a need to electrify a variety of historically fossil-fuel intensive heating processes, many of which require reaction temperatures above 500°C. In the chemicals industry, fluidized beds are often used in chemical reactors due to enhanced heat and mass transfer properties compared to a fixed bed [1] - [3]. Compared to several other electric heating technologies, magnetic induction enables wireless, volumetric internal heating capabilities and can readily scale in volume and power. Properly designed system configurations can achieve close to unity power-to-internal heat conversion. Fig. 1(a) shows a generic cross-section of an inductively heated fluidized bed, where conductive particles are fluidized with gas flowing up from the bottom of the reactor. The fluidized conductive particles serve as the susceptor for internal reactor heating, and they form a random, dynamically reconfiguring conductive network that can be collectively described as a homogenized medium with an effective electrical conductivity. An AC current is injected into the helical coil at some frequency to create an alternating axial magnetic field, which generates eddy currents within the fluidized bed. This in turn generates joule heat within the bed. Tailoring the operating frequency to the susceptor's conductive properties allows for efficient and volumetric wireless power transfer [4]. Described in the next section, maximum power transfer in our system occurs in the MHz range as the relative power delivery to the fluidized bed component of the total load is maximized.

A Class-E amplifier is a single-switch resonant amplifier that can achieve high efficiency at MHz due to the following: (1) it requires simple gate drive with a low-side switch (2) it incorporates the transistor capacitance into the input network to shape the voltage during the off period of the transistor to (3) achieve zero-voltage switching (ZVS) during transistor turn-on [5]. In Section III we discuss the design criteria of a 13.56 MHz Class-E amplifier to power a fluidized bed.

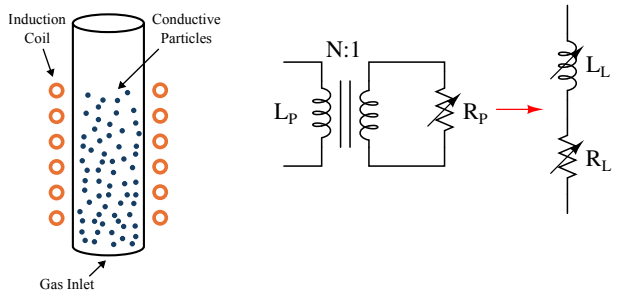

Fig. 1: (a): A graphical depiction of a six turn inductively heated fluidized bed. (b): A generalized narrowband circuit transformation of an inductively heated varying load, neglecting coil resistance and leakage inductance.

II. Fluidized Load

To determine the operating frequency of any inductively heated system, we must perform an AC resistance sweep of the system looking into the coil and susceptor across some frequency band to evaluate the coupling efficiency. Separate from the power amplifier efficiency, the coupling efficiency of the system η_{coup} is frequency-dependent and defined as the percentage of output power injected into the magnetic coil that is delivered to the effective resistance of the fluidized media R_{susc} (and not dissipated in the coil resistance R_{coil}). Fig. 2 illustrates the time-averaged AC resistance characterization of our fluidized graphite bed and the coupling efficiencies under different regimes of fluidization up to nitrogen gas flow rates of 20 slpm. The AC resistance trends of the bed indicate that it can be effectively modeled as a homogeneous cylinder with an effective conductivity that decreases as the gas flow rate increases. The highest coupling efficiency occurs near the ISM band of 13.56 MHz, which we chose to operate our power amplifier at. Frequencies above this result in less magnetic

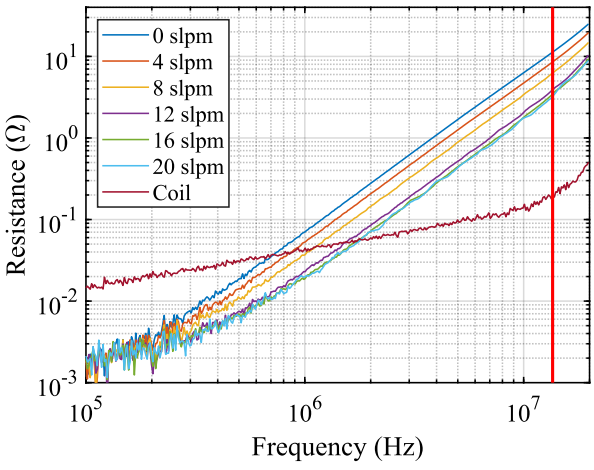

(a)

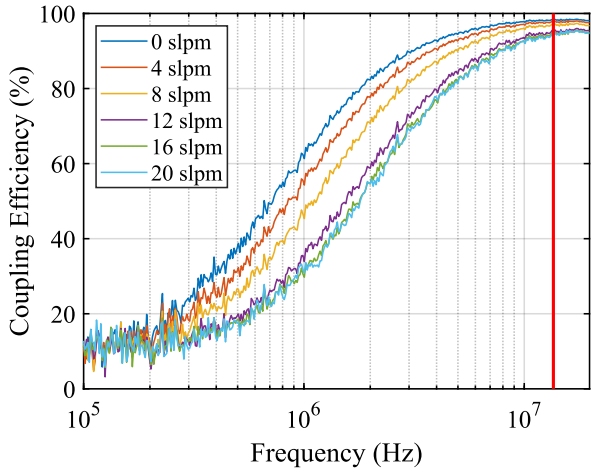

(b)

Fig. 2: (a): Experimentally measured AC resistance of the fluidized bed as a function of frequency and nitrogen gas flow rate. The AC resistance of the induction coil alone is also plotted. The red line marks 13.56 MHz. (b): Coupling efficiency as a function of frequency and gas flow rate.

field penetration, leading to less uniform heating. Put simply, the coupling efficiency does not increase further beyond this point, leading to diminishing returns in heating profile.

$$\eta_{coup} = \frac{R_{susc}}{R_{susc} + R_{coil}} \tag{1}$$

Because the graphite particles in the fluidized bed are in motion, the electrical properties of the fluidized bed as observed during induction heating temporally vary at all frequencies. While in general the bed can be treated as a single medium with an effective conductivity related to the volume fraction and fluidization state of the particles [6], the rapid changes in effective conductivity, and thus effective impedance, pose a challenge when trying to heat the bed. Unfortunately, the conventional Class-E amplifier's efficiency is highly sensitive to load variation, which necessitates accurate characterization of the load impedance and design reconsideration of the amplifier topology to handle the load variance.

One could look toward digital controls techniques to sense changes in the output load through voltage or current sensing at the output and respond accordingly through gate drive control. However, since our system operates at 13.56 MHz, current state of the art microcontrollers do not have the sensing, timing, and processing speed to adjust the gate signals to maintain ZVS for fast load transients. Thus, we must look toward passive circuit solutions to compensate for such load variations.

The load (the induction coil and fluidized bed) is modeled as a series varying resistance and varying inductance for power amplifier design. However, the load can equivalently be modeled as a constant inductance in parallel with a varying resistance seen through a transformer, where the resistance is varying due to the motion of the particles (Fig. 1(b)). Using the fact that L_p is a constant, from Fig. 1 we can equate the parallel and series load models to find a closed-form parametric relationship as a function of R_p between R_L and L_L in the series model to support amplifier design.

$$\frac{1}{\frac{1}{jwL_P} + \frac{1}{N^2 R_P}} = \frac{w^2 L_P^2 N^2 R_P + jwL_P N^4 R_P^2}{N^4 R_P^2 + w^2 L_P^2} = R_L + jwL_L \tag{2}$$

$$R_L = \frac{w^2 L_p^2 N^2 R_p}{N^4 R_p^2 + w^2 L_p^2} \quad L_L = \frac{L_p N^4 R_p^2}{N^4 R_p^2 + w^2 L_p^2} \tag{3}$$

Experimental knowledge of where on the parametric curve the system operates guides the design of the amplifier towards load invariance. In our system, the relationship between L_L and R_L is well approximated linearly. Fig. 3 shows load impedance data captured over two minutes with a VNA (Bode 100) at our operating frequency of 13.56 MHz and a nitrogen gas flow rate of 16 slpm.

TABLE I: Fluidized Bed Load Impedance Range

Element	Minimum	Average	Maximum
R_L	5.24Ω	6.33Ω	7.42Ω
L_L	1.471 μH	1.480 μH	1.488 μH

III. Power Amplifier Design

Due to the switching frequency of our amplifier, a passive solution for maintaining ZVS is required, thus design equations for a variable load single-switch inverter from [7] are used. However, our load has a significant inductance whereas an ideal load for this design would be purely resistive. A simple approach to manage the inductance of the load would be to add a capacitor C_M resonant with the average value of L_L. However, the small value of R_L causes high currents throughout the circuit and high conduction losses in the switch, limiting efficiency and power output. Thus, we design the amplifier to include a C-C matching network to transform the average load impedance to an effective value of 50 Ω (Fig. 4).

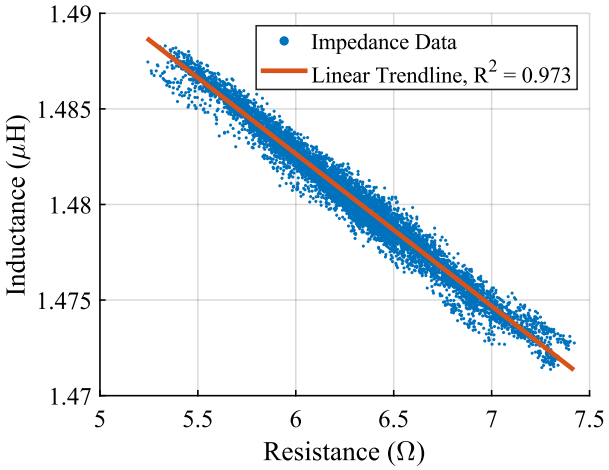

Fig. 3: Experimental capture of series resistance R_L and series inductance L_L in the fluidized bed load at 13.56 MHz.

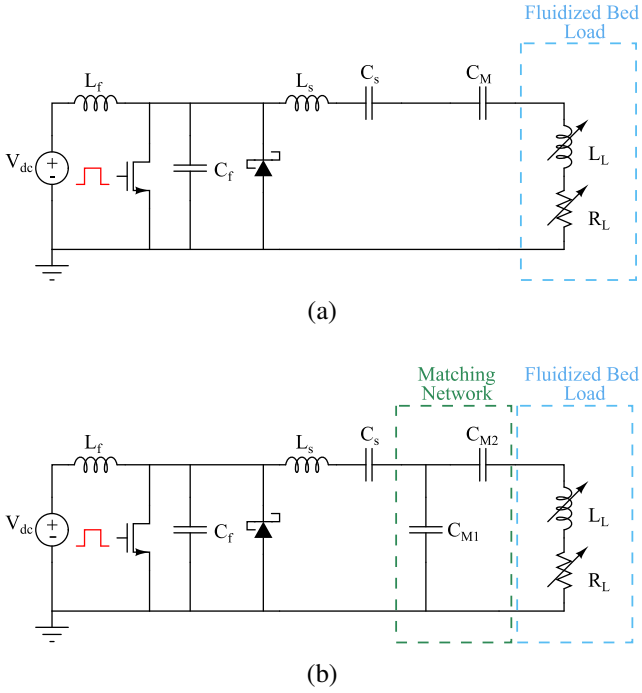

Fig. 4: (a): Schematic of load-invariant Class-E amplifier with series reactance cancellation. (b): Schematic of load-invariant Class-E amplifier with C-C output matching network.

From [7], L_f and C_f are designed according to the minimum load resistance R_{min} and the switching frequency f_{SW}. Thus, we use the lowest resistance seen looking into the matching network over the fluidized bed impedance range for R_{min}. We choose a value of $k_f = 0.7$.

$$C_f = \frac{1}{3\pi f_{SW} k_f R_{min}} \tag{4}$$

$$L_f = \frac{k_f R_{min}}{3\pi f_{SW}} \tag{5}$$

While stepping up the effective load resistance more would further decrease conduction loss, there is a limit as R_{min} is inversely proportional to C_f, and C_f must be large enough to accommodate the transistor's output capacitance and additional tuning required to optimize for output capacitance nonlinearities. A high step-up ratio also requires a more precise and thus difficult tuning implementation. Furthermore, when choosing a transistor, drain-source on-resistance and thus resistive losses will increase with decreasing output capacitance.

The most important priority for this application is to maximize output power, rather than compromising power in exchange for features like improved output harmonic distortion. This is due to the high temperature requirements for heat-intensive chemical manufacturing processes and the low consequences of distortion in induction heating. A lower-range Q value of $Q = 3$ is chosen for the series output network L_S and C_S, as the matching network also will add attenuation of higher order harmonics.

IV. Matching Network

We aim to design a matching network that increases the resistive load as seen by the amplifier and handles both resistive and reactive load variation. There are several ways to handle this: impedance compression networks and tunable matching networks (TMNs). ICNs require two loads or two coils; TMNs are slow and do not serve our need for high speed controls [8] [9]. Furthermore, since the load must appear resistive to maintain ZVS [7], we aim to choose a matching network that minimizes phase angle across the load range. A C-C matching network has low part count and provides phase angle compression looking into the matching network as the load varies.

Fortunately, since the relationship between L_L and R_L is approximately linear, the matching network can be designed to minimize output reactance (equivalently phase angle) looking into the network over the impedance profile. For the desired (purely resistive) nominal matched impedance R_S at the average L_L and R_L, we can find C_{M1} and C_{M2}:

$$Q_M = \sqrt{\frac{R_S}{R_{L_{avg}}} - 1} \tag{6}$$

$$C_{M1} = \frac{Q_M}{\omega R_S} \quad C_{M2} = (\omega^2 L_{L_{avg}} - Q_M \omega R_{L_{avg}})^{-1} \tag{7}$$

The goal is to find R_S that minimizes the average phase angle magnitude across the load range:

$$\frac{1}{R_{L_{max}} - R_{L_{min}}} \int_{R_{L_{min}}}^{R_{L_{max}}} \tan^{-1}\left(\frac{\mathrm{Im}\{Z_M\}}{\mathrm{Re}\{Z_M\}}\right) dR_x \tag{8}$$

Where Z_M is the impedance looking into the matching network, and L_x is calculated from the equation of the load

impedance profile regression line from Fig. 3, with L_0 and R_0 being the y and x-intercepts respectively:

$$Z_M = \frac{1 - w^2 C_{M2} L_x + jwC_{M2} R_x}{-w^2 R_x C_{M1} C_{M2} + jwC_{M1}(1 + \frac{C_{M2}}{C_{M1}} - w^2 L_x C_{M2})} \tag{9}$$

$$L_x = \left(\frac{L_0}{R_0}\right) R_x + L_0 \tag{10}$$

Using the optimal value of $R_S = 78\,\Omega$, the average reactance looking into the C-C matching network is significantly reduced as compared to simply adding a series capacitor to resonate with the average L_L (Fig. 5). The C-C matching network has a mean phase distortion magnitude of 0.37° and standard deviation of 0.28°, while a series capacitor introduces a mean of 3.38° with a standard deviation of 2.02°.

While the optimal value of R_S is $78\,\Omega$, we chose $R_S = 50\,\Omega$ due to the difficulty in tuning C_f with increasing R_S as discussed in Section III. This introduces a mean phase distortion magnitude of 0.76° and standard deviation of 0.57°.

V. Experimental Results

During preliminary experiments using purely series reactance cancellation, power output was limited to 25 W due to transistor overheating. This was due to two reasons: the low load resistance led to high input currents into the system and thus high conduction losses in the transistor. Additionally, the amplifier had significant phase angle variation at the output and thus non-ZVS switching. As such, we implemented the C-C matching network to tackle both problems to achieve load invariance and higher power operation.

With the addition of the C-C network tuned for a 50 Ω load, we operated the 13.56 MHz amplifier at 66.5 V with a maximum power of 115 W delivered to the load. Across a ten minute heating test, we did not observe any non-ZVS waveforms, indicating the amplifier was invariant to any impedance variation of the fluidized bed, as shown in Fig. 7(a). In 7(b), the output of the amplifier is also shown, indicating low harmonics. The transistor reached a maximum temperature of 60.6°C (Fig. 8), indicating that the amplifier can push to higher powers. The 300 μm graphite flakes, fluidized with 16 slpm of nitrogen gas in a 2-inch quartz tube reactor (Fig. 9), were inductively heated from 23°C to 100°C as measured by thermal camera (FLIR A655sc). (Fig. 10) We can further increase the temperature of the bed in future experiments with insulation. We used a directional coupler (Werlatone C3807) connected to a power meter (Keysight N1914A) through power sensors (Keysight N8482A) to measure the RF power output. The amplifier had a maximum efficiency of 92% at the nominal effective load value of 50 Ω (Fig. 11).

VI. Conclusion

This paper presents the design and experimental operation of a 115 W load-invariant Class-E amplifier to inductively heat a fluidized bed at 13.56 MHz. After characterization of the load impedance profile, a C-C matching network transforms

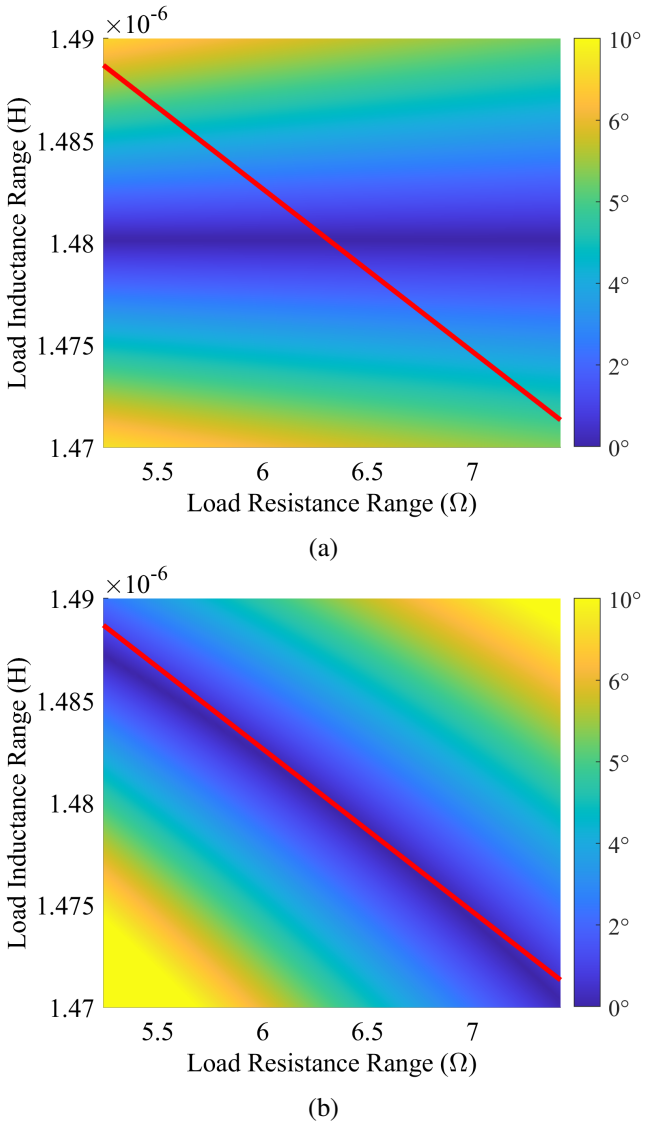

Fig. 5: Comparison of phase angle magnitude between matching network topologies for an average effective transformed load of $78\,\Omega$. The fluidized bed load impedance regime is marked by the red line. (a) Series network phase angle magnitude. (b) C-C network phase angle magnitude.

TABLE II: Power Amplifier Components List

Component	Board Value and Description
L_f	0.22 μH, 2 turns, 10 AWG
C_f	53 pF, C0G, 1kV
Switch	Infineon GS-065-030-2-L, 650V, 20A
Gate Driver	Texas Instruments LMG1025-Q1
Antiparallel Diode	STMicroelectronics STPSC406, 600V, 40A
L_S	1.41 μH, 7 turns, 10 AWG
C_S	97 pF, C0G, 1kV
C_{M1}	618 pF, C0G, 1kV
C_{M2}	101 pF, C0G, 2kV

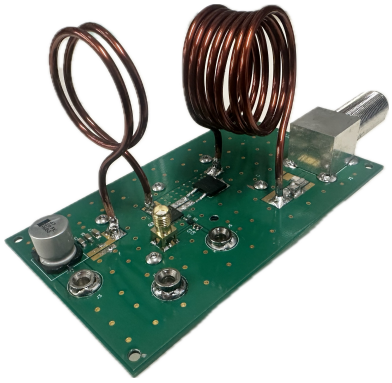

Fig. 6: Class-E amplifier board (with heat sink mounted underneath transistor).

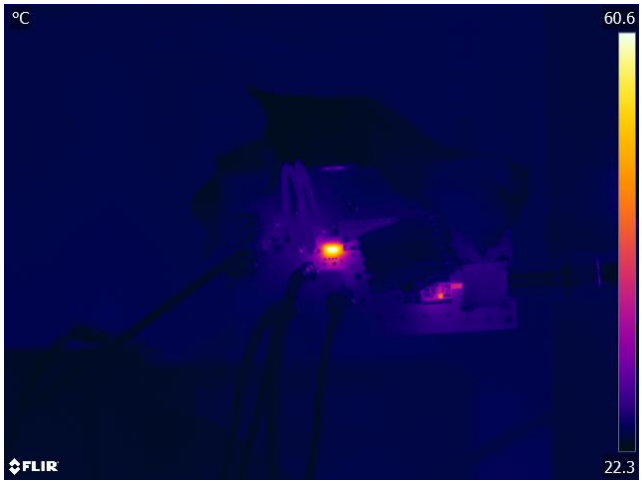

Fig. 8: Thermal image of the amplifier during continuous operation at 115 W output power.

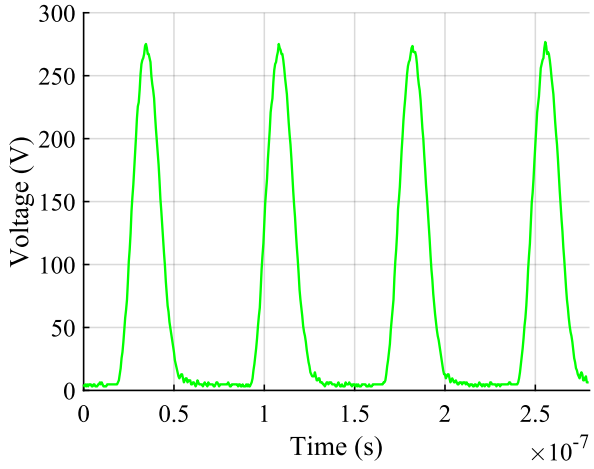

(a)

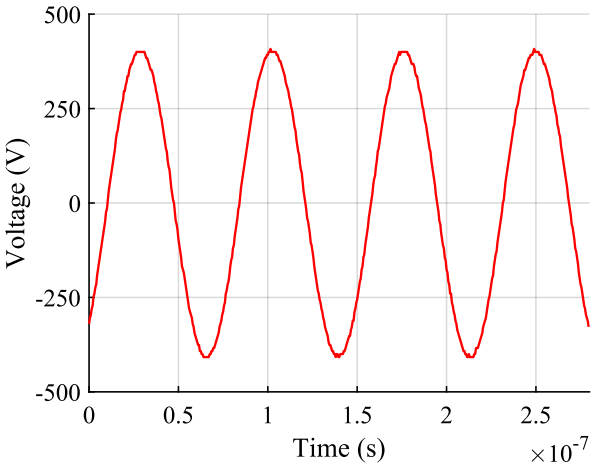

(b)

Fig. 7: (a) Measured drain voltage at 115 W output power. (b) Measured load (induction coil and fluidized bed) voltage at 115 W output power.

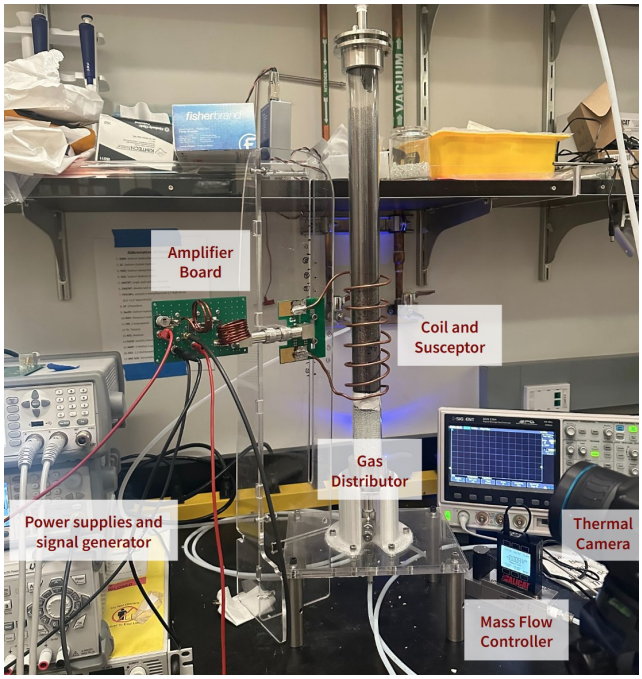

Fig. 9: Small scale quartz tube fluidized bed reactor with Class-E amplifier powered induction coil.

the average impedance of the varying load to 50 Ω. This decreases input current and compresses output network phase angle variation, thus maintaining ZVS across the load range and enabling high efficiency, high power operation. At 115 W, the amplifier has a measured drain efficiency of 92% at the nominal transformed load resistance. We present a high-frequency resonant power amplifier geared towards the electrification of fluidized bed reactors in heavy industry.

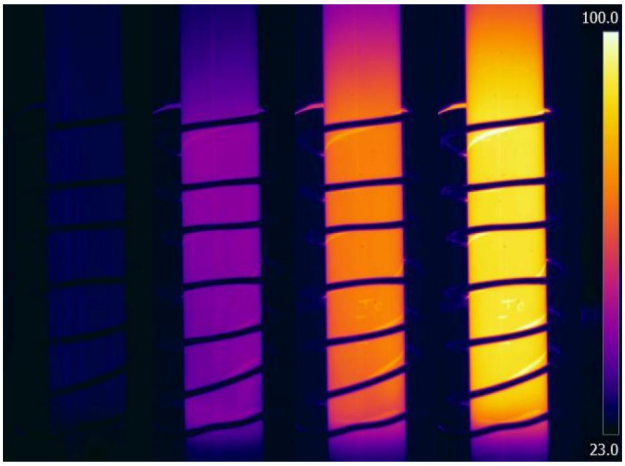

Fig. 10: Thermal images of the fluidized graphite bed heated from 23°C to a maximum temperature of 100°C.

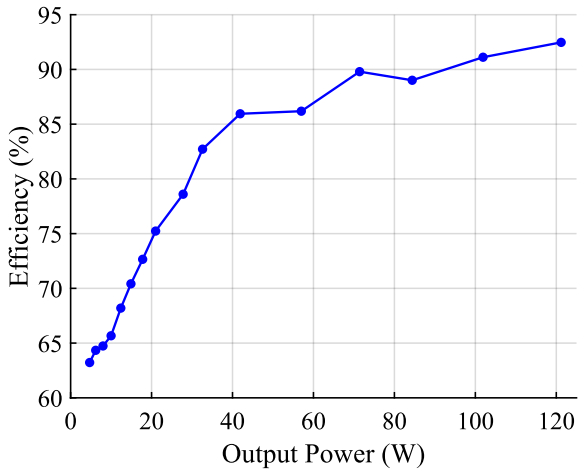

Fig. 11: Power amplifier efficiency across output power with the nominal load of 50 Ω looking into the matching network.

REFERENCES

[1] R. Cocco, S. B. R. Karri, and T. Knowlton, "Introduction to Fluidization," Chemical Engineering Progress, vol. 110, no. 11, pp. 21-29, Nov. 2014.

[2] V. V. Idakiev, P. V. Lazarova, A. Bück, E. Tsotsas, and L. Mörl, "Inductive heating of fluidized beds: Drying of particulate solids," Powder Technology, vol. 306, pp. 26–33, 2017.

[3] I. Ahmed, M. Duchesne, Y. Tan, and D. Y. Lu, "Electrically heated fluidized beds - A review," Industrial & Engineering Chemistry Research, vol. 63, no. 10, pp. 4205–4235, 2024.

[4] C. H. Lin et al., "Electrified thermochemical reaction systems with high-frequency metamaterial reactors," Joule, vol. 8, no. 10, pp. 2938-2949. Oct. 2024, doi: 10.1016/j.joule.2024.07.017

[5] N. O. Sokal, "Class-E RF power amplifiers," QEX, vol. 204, no.1, pp. 9-20, Jan. 2001.

[6] E. Rognin, G. Barbarossa, P. Brun, J. Lacombe, and E. Sauvage, "Computation of eddy currents in highly conductive particles dispersed in a moderately conductive matrix," International Journal of Applied Electromagnetics and Mechanics, vol. 53, 2017, doi: 10.3233/JAE-162241

[7] L. Roslaniec, A.S. Jurkov, A. Al Bastami and D.J Perreault, "Design of single-switch inverters for variable resistance/load modulation operation," IEEE Transactions on Power Electronics, vol. 30, no. 6, pp. 3200-3214, June 2014, doi: 10.1109/TPEL.2014.2331494

[8] J. Choi, J. Xu, R. Makhoul and J. M. R. Davila, "Implementing an Impedance Compression Network to Compensate for Misalignments in a Wireless Power Transfer System," in IEEE Transactions on Power Electronics, vol. 34, no. 5, pp. 4173-4184, May 2019, doi: 10.1109/TPEL.2018.2862414.

[9] C. Hoarau, N. Corrao, J. . -D. Arnould, P. Ferrari and P. Xavier, "Complete Design and Measurement Methodology for a Tunable RF Impedance-Matching Network," in IEEE Transactions on Microwave Theory and Techniques, vol. 56, no. 11, pp. 2620-2627, Nov. 2008, doi: 10.1109/TMTT.2008.2006105.